Materials Characterization 115 (2016) 39–45

Contents lists available at ScienceDirect

Materials Characterization

journal homepage: www.elsevier.com/locate/matchar

Discontinuous precipitates in age-hardening Cu—Ni—Si alloys

Satoshi Semboshi [a,*], Shigeo Sato [b], Akihiro Iwase [c], Takayuki Takasugi [c]

[a] Kansai Center, Institute for Materials Research, Tohoku University, 1-1 Gakuen-cho, Naka-ku, Sakai, Osaka 599-8531, Japan
[b] Graduate school of Science and Engineering, Ibaraki University, 4-12-1 Nakanarusawa, Hitachi, Ibaraki 316-8511, Japan
[c] Department of Materials Science, Osaka Prefecture University, 1-1 Gakuen-cho, Naka-ku, Sakai, Osaka 599-8531, Japan

ARTICLE INFO

Article history:
Received 11 February 2016
Received in revised form 16 March 2016
Accepted 17 March 2016
Available online 25 March 2016

Keywords:
Cu alloy
Discontinuous precipitation
Aging
Hardening
Microstructure
Electron diffraction

ABSTRACT

The microstructural evolution and characterization of discontinuous precipitates in a Cu-4.3 Ni-2.2 Si (in at.%) alloy were studied, and compared with those of continuous precipitates in the same alloy. During prolonged aging, coarse cellular components containing fiber-shaped δ-Ni_2Si and copper solid-solution phases nucleate and grow quickly but discontinuously at the grain boundaries, accompanied by the consumption of fine δ-Ni_2Si particles formed by continuous precipitation. In terms of the crystal structure, all the precipitates are of the same type of orthorhombic δ-Ni_2Si. However, in terms of the crystallographic features, the δ-Ni_2Si discontinuous precipitates have micro-scale fibers that are aligned with the orientation relationship of $\langle 100\rangle_\delta // \langle 110\rangle_{Cu}$ and $(013)_\delta // (1\bar{1}1)_{Cu}$, and with a preferential extending direction on the $(111)_{Cu}$ plane, which differs from the fine δ-Ni_2Si continuous precipitates at the early stages of aging. The evolution of the discontinuous precipitates can be explained by the existing classical theories of phase transformation, as discussed by Hu et al. regarding the subsequence of the continuous precipitates. In this study, we also confirmed that the development of coarse δ-Ni_2Si discontinuous precipitates of the cellular components leads to a serious drop in the strength in the later stages of aging.

1. Introduction

Corson-type alloys based on Cu—Ni—Si have gained considerable industrial significance given their extensive application to electrical devices, such as lead frames and electrical connectors, because of their excellent combination of electrical conductivity and strength [1–4]. The alloys are commercially manufactured through a conventional aging procedure. Cu—Ni—Si alloys, containing <5 at.% Ni and 2.5 at.% Si at an Ni/Si ratio of around 2.0, are solution-treated at temperatures in excess of 1123 K and then quenched in water, followed by aging at temperatures between 673 K and 773 K, based on the Cu—Ni_2Si pseudo-binary phase diagram shown in Fig. 1 [5]. This procedure yields an age-hardening effect, due to the formation of Ni—Si precipitates in the Cu matrix.

The precipitating phase responsible for the age-hardening has been investigated by a number of researchers, especially regarding the early stages of aging [6–15]. To date, the age-hardening precipitates in the alloys have been widely accepted as being δ-Ni_2Si intermetallics with an orthorhombic structure [6–17], although other types of precipitates, such as β-Ni_3Si, $(Cu,Ni)_3Si$, and other metastable phases, might coexist [8,12–15]. In their most recent study, Hu et al. investigated the subsequent age-hardening of δ-Ni_2Si precipitates (i.e., continuous precipitates (CPs)) that form during isothermal aging, and explained their behavior using classical theories of phase transformation in association with energy calculations [14]; the CPs in Cu-2.6 Ni-1.6 Si-0.5 Cr (in at.%) alloys did not exhibit any changes in their δ-Ni_2Si crystal structure, but underwent changes in their morphology and other crystallographic features. There were basically two types of δ-Ni_2Si precipitates in the alloys, namely, δ_1-Ni_2Si and δ_2-Ni_2Si. In the early stages of aging, disk-shaped δ_1-Ni_2Si precipitates, several nanometers in diameter, were continuously nucleated in the parent super-saturated solid-solution phase, and had an orientation relationship (OR) with the Cu matrix: $\langle 010\rangle_{\delta 1} // \langle 110\rangle_{Cu}$ and $(001)_{\delta 1} // (001)_{Cu}$. In the latter stages of aging, the δ_1-Ni_2Si precipitates grow to several tens of nanometers in diameter, with a slight rotation, and then transform to cigar-shaped δ_2-Ni_2Si precipitates with an OR of $\langle 100\rangle_{\delta 2} // \langle 011\rangle_{Cu}$ and approximately $(013)_{\delta 2} // (1\bar{1}1)_{Cu}$. Thus, the continuous precipitates subsequently develop as follows: supersaturated solid solution → δ_1 → δ_1 (rotated) → δ_2.

For the later stages of aging in some age-hardenable Cu alloys, coarse cellular components consisting of the stable intermetallic phase (i.e., discontinuous precipitates (DPs)) and the terminal solid solution phase are often formed at grain boundaries, because grain boundary diffusion rather than volume diffusion is expected to be a dominant mechanism of constituent element transport at low aging temperatures

* Corresponding author at: Institute for Materials Research, Tohoku University, 1-1 Gakuen-cho, Naka-ku, Sakai, Osaka 599-8531, Japan.
E-mail addresses: semboshi@imr.tohoku.ac.jp (S. Semboshi), shigeo.sato.ar@vc.ibaraki.ac.jp (S. Sato), iwase@mtr.osakafu-u.ac.jp (A. Iwase), takasugi@mtr.osakafu-u.ac.jp (T. Takasugi).

http://dx.doi.org/10.1016/j.matchar.2016.03.017
1044-5803/

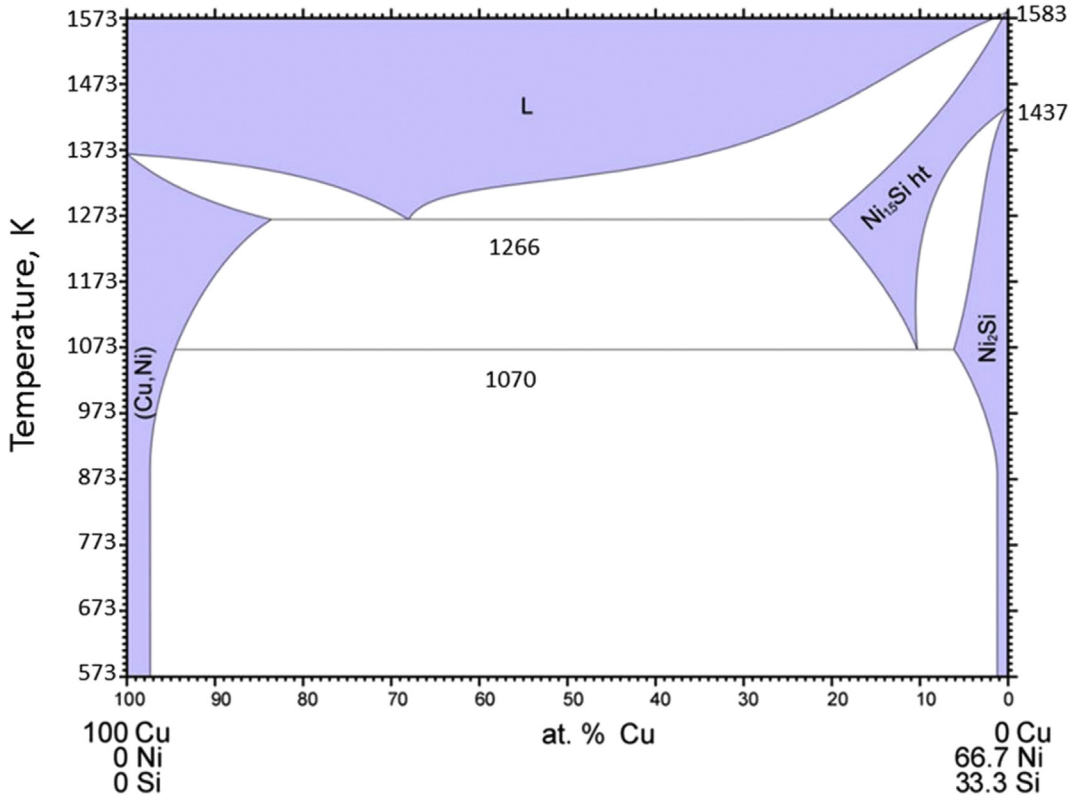

Fig. 1. Phase diagram of Cu–Ni2Si pseudo binary system [5].

[18–21]. For Cu—Ni—Si based alloys, it was found that micro-scaled DPs nucleate at the grain boundaries during prolonged aging, competing with the gradual growth of the nano-scaled δ-Ni_2Si continuous precipitates (CPs) [22–24]. To investigate the evolution and nature of the DPs, as well as the CPs, is important, because it is generally recognized that the development of cellular components containing coarse DPs is well known to result in a significant decrease in age-hardening [19,20]. However, there has been very little research that would aid in understanding of the characteristics of the coarse DPs in Cu—Ni—Si alloys. In this study, the discontinuous precipitation behavior, including the structure, morphology, crystallographic orientation relationship and evolution, of a commercial alloy with a nominal composition of Cu-4.3 Ni- 2.2 Si (at.%) was investigated, and compared with those of the CPs in the same alloy. The influence of DPs on the microstructural evolution of the aged alloys was correlated with variations in the hardness and electrical conductivity.

2. Materials and methods

An alloy ingot with a chemical composition of Cu-4.3 Ni-2.2 Si in at.% (Cu-4.1 Ni-0.97 Si in wt.%) was provided by YAMATO ALLOY Co., Ltd. From this ingot, blocks measuring 30 mm × 30 mm × 3 mm were cut off, and then cold-rolled down to a thickness of 0.3 mm. From the resulting rolled sheet, strips measuring 75 mm × 5 mm × 0.3 mm were cut off. The specimens were solution-treated at 1173 K for 3 h in evacuated quartz capsules, and then immediately quenched in water. The contaminated layer on the specimen surface was removed by mechanical grinding. The specimens were then re-capsulated in a vacuum, followed by isothermal aging at 723 K for 1 to 720 h.

The aging behavior of the specimen was monitored by measuring the Vickers hardness and electrical conductivity. The Vickers hardness tests were conducted by applying a load of 1.96 N, and the hardness values were then determined by averaging the values from >10 indentations. The electrical conductivity was measured at room temperature by using a standard DC four-probe technique with a micro-ohm meter with an accuracy of ± 10 μΩ. The microstructures of the specimens were observed using a JEOL JSM7001F field emission scanning electron microscope (FESEM) operating at 15 kV and a JEOL JIM-3010 transmission electron microscope (TEM) operating at 300 kV. For the FESEM observations, the specimens were mechanically polished and then chemically etched with a 7-mol/L nitric acid-water solution at 273 K for 10 s. For the TEM observations, thin foil-like specimens were prepared by mechanically grinding the specimen to a thickness of <30 μm, followed by low-angle ion milling using an argon ion beam accelerated by a voltage of up to 3 kV. High-purity argon gas (99.99999 vol.%) was used as the argon ion-beam source. The volume fraction of the cellular components consisting of DPs and solid solution were measured from the FESEM images, which was obtained by a point counting method on a total scanning area of >4 mm^2.

The precipitates formed in the aged specimens were separated using the following extraction procedure [25]. First, the surfaces of the aged specimens were ground again to remove any contamination. After the samples had been thoroughly rinsed in pure ethanol, they were cut into small pieces measuring <1 mm × 1 mm × 0.3 mm, which would easily dissolve. These pieces were submerged in a 7-mol/L nitric acid–water solution at 273 K and then stirred in an ultrasonic bath for approximately 20 min. After this procedure, only the copper matrix phase dissolved in the solution, but the Ni and Si-rich precipitates remained as insoluble residue. The solution was then passed through a membrane filter with a pore diameter of 0.05 μm. The filtered precipitates were rinsed well with pure water and then dried in a desiccator. To determine the structure of the insoluble precipitates, X-ray diffraction (XRD) analysis was performed using a PANalytical X'Pert Pro diffractometer with CuKα radiation at 40 kV. The mass fractions of the elemental Cu, Ni, and Si in the insoluble precipitates were measured by inductively coupled plasma-optical emission spectrometry (ICP-OES) performed using a Thermo Fisher Scientific IRIS Advantage DUO

spectrometer, and then determined by averaging the values from more than three measurements.

3. Results and discussion

3.1. Microstructural evolution of DPs

The solution-treated (as-quenched) specimen prepared in this study exhibits a single phase microstructure of a supersaturated solid solution of Cu, with grain sizes of <100 μm. Fig. 2 shows FESEM and TEM microstructure images of the specimens aged at 723 K in the early aging period, that is, after the first 2 h. At this point, there are not yet any cellular components containing discontinuous precipitates (DPs) at the grain boundaries of the specimen (Fig. 2(a)). On the other hand, continuous precipitates (CPs) with a size of <1 nm are formed in the matrix phase, as shown in the bright-field TEM image viewed from the $\langle 001\rangle_{Cu}$ direction (Fig. 2(b)). Based on the TEM observations viewed from different incident beam angles, the CPs were confirmed as having a disk-like shape. The selected area electron diffraction (SAED) pattern taken from the region observed in Fig. 2(b) is shown in Fig. 2(c). The extra spots and streaks in the SAED pattern shown in Fig. 2(c) can be assigned to the ordered δ-Ni_2Si with an orthorhombic structure [13,14]. We can identify, therefore, that the fine disk-shaped CPs are composed of a δ-Ni_2Si phase. Figs. 2(b) and (c) also show that the disk-shaped CPs lie on the $\{110\}_{Cu}$ planes. The orientation relationship between the matrix and fine continuous precipitate phases was $\langle 010\rangle_{\delta 1}$// $\langle 110\rangle_{Cu}$, and $(001)_{\delta 1}$//$(001)_{Cu}$. These crystallographic features agree with those reported previously [13,14].

Fig. 3 shows the microstructural subsequence of the specimens aged at 723 K for 4 h, 16 h, and 240 h. After aging for 4 h (Fig. 3(a)), some grains exhibit cellular components containing coarse DPs, as indicated by the black arrows, although the majority of the grains do not have any DPs but rather contain fine-scaled CPs. Thus, the DPs nucleate preferentially at the grain boundaries, resulting in a heterogeneous microstructure. If we view the series of Figs. 3(a) to (c), it is evident that the volume fraction of the grains occupied by the cellular components increases with the aging time, thus replacing the sound grains containing fine-scaled CPs of δ-Ni_2Si. Fig. 4 shows the change in the volume fractions of the cellular components with aging time. The volume fractions of the cellular components start to increase after aging for 4 h, eventually reaching a value in excess of 95% after 120 h.

The shape of the DPs in the cellular components is fiber-like, being several tens of nanometers in diameter and several μm in length, as shown in the magnified FESEM image in the inset in Fig. 3(a). The shape and size of the DPs do not appear to be significantly changed even after aging for 240 h (see Fig. 3(c)'), whereas the CPs grow in size from <1 nm to several tens of nanometers with the elapse of aging time (Fig. 3(c)"), which is in good agreement with the literature [9,14]. It is interesting that the fiber-shaped DPs entirely occupy the individual grains even if the aging progresses only for a short period from 2 h to 4 h (Fig. 3(a)). This suggests that once the DPs nucleate at a grain boundary facet, they extend very quickly over an entire grain. This can be explained by the one-dimensional growth of the fiber, which will progress more quickly than with conventional two-dimensional (i.e., laminated-shaped) and three-dimensional discontinuous precipitates, as seen in many other copper alloys [18–21]). Therefore, it is proposed that the kinetics of the DPs in the alloys is controlled by the nucleation reaction at the grain boundaries rather than by the growth reaction in the grain interior.

It should be noted that the initiation of the discontinuous reaction is not homogeneous at all of the grain boundaries. This implies that the nucleation of the DPs may be subject to the characteristics of the grain boundaries, such as the grain boundary energy and the crystal orientation of the matrix along the grain boundaries, which will report on in the future.

3.2. Characterization of DPs

To identify the structure and composition of the DPs in the above-mentioned specimens, the precipitates in the fully aged specimen were separated from the matrix by using an extraction technique. Fig. 5 shows the appearance of the insoluble residue extracted from a specimen aged at 723 K for 240 h. Here, it is supposed that the specimen aged 240 h is in the equilibrium state, because the microstructural evolution and the variations in the hardness and electrical conductivity do not progress any more, as shown in Fig. 4 and Fig. 8 (the latter figure will be discussed in the next session). We can see fiber-shaped residues measuring <100 nm in diameter and several μm in length, whose features are identical to those of the DPs shown in Fig. 3(c)'. Consequently, the observed fibers can be confirmed as being the DPs contained in the cellular components. It was difficult to find disk-shaped residue of the CPs in Fig. 5, because their volume fraction was somewhat smaller than that of the DPs in the specimen aged for 240 h (Figs. 3 and 4).

Fig. 6 shows the XRD profile of the DPs extracted from the specimen aged at 723 K for 240 h. We detected no peaks corresponding to copper, indicating that the entire solid-solution matrix phase of the copper had dissolved in the nitric acid solution. The XRD profile exhibited peaks corresponding to δ-Ni_2Si with an orthorhombic structure in the spacing group of *Pnma*. Fig. 6 also shows a fitting pattern calculated by Rietveld analysis for the δ-Ni_2Si compound (open circles), with the difference between the measured and calculated intensities at the bottom. These suggest that the calculated pattern for the δ-Ni_2Si is in good agreement with the measured results. This is supported by the fact that the indicator of the accuracy of the Rietveld fitting, *S*, was 1.64, thus indicating

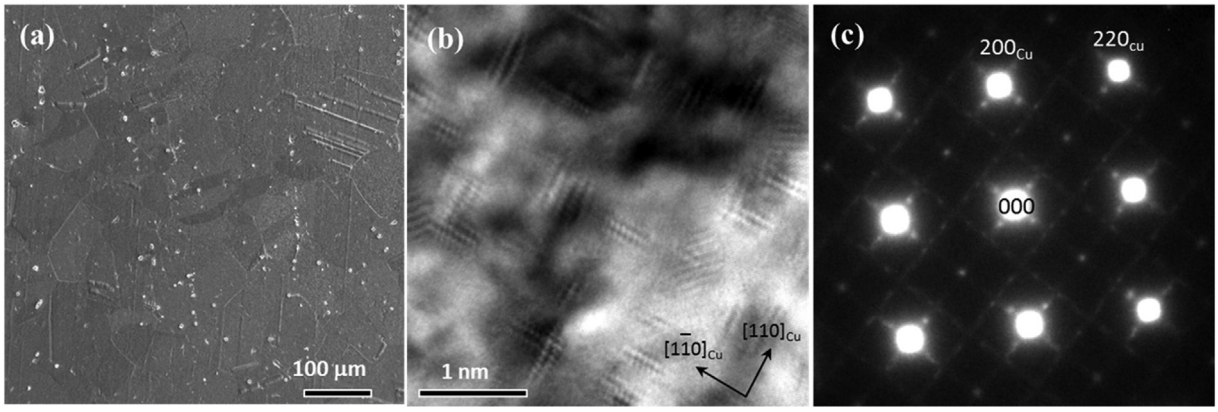

Fig. 2. FESEM image (a), bright-field TEM image (b) and corresponding selected area electron diffraction (SAED) pattern (c) of Cu-4.3 at.% Ni-2.2 at.% Si alloy specimens aged at 723 K for 2 h.

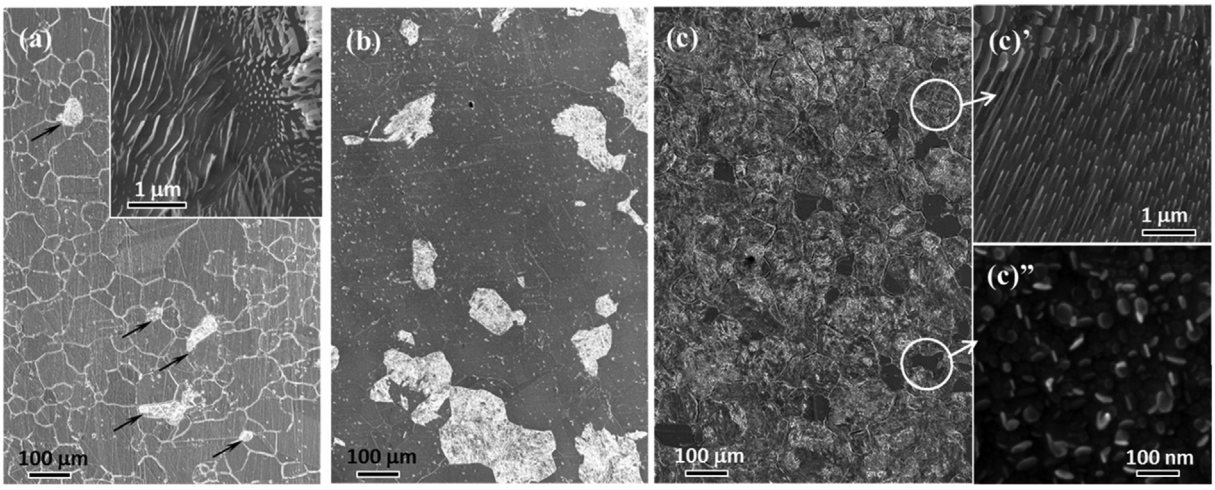

Fig. 3. FESEM images of Cu-4.3 at.% Ni-2.2 at.% Si alloy specimens aged at 723 K for 4 h (a), 16 h (b), and 240 h (c), together with magnified FESEM images (insets). The black arrows in (a) indicate cellular components containing coarse discontinuous precipitates.

that the Rietveld analysis had a high level of reliability [26]. We can therefore conclude that the DPs were identified as being δ-Ni_2Si, i.e., both the CPs and DPs have the same crystal structure. Hereafter, the δ-Ni_2Si generated in the discontinuous precipitation manner is referred to as δ_D-Ni_2Si. Table 1 summarizes the lattice parameters determined by the Rietveld analysis for the fiber δ_D-Ni_2Si extracted from the specimen aged at 723 K for 240 h, together with those for pure δ-Ni_2Si intermetallic compound [16,17] and δ-Ni_2Si formed in the CP manner [13]. The lattice parameters for the δ_D-Ni_2Si were the same as those formed in the CP manner within the limits of experimental accuracy.

The chemical composition and mass fractions of both the DP and matrix phases could be analyzed directly by performing the extraction and then ICP-OES measurements. Table 2 lists the results for the Cu—Ni—Si alloy specimen aged for 240 h. The concentrations of Cu, Ni, and Si in the precipitates was 0.77 at.%, 62.15 at.%, and 37.07 at.%, respectively; the δ_D-Ni_2Si contains a small amount of copper, and the measured Ni/Si ratio was 1.68, which is slightly different from the stoichiometric composition of 2.0 (the Ni/Si atomic ratio may be somewhat closer to 5/3). In the matrix phase of the specimen, aged for a prolonged period of 240 h, the concentration of Si was nearly zero, whereas a small amount of Ni was found to remain. The fraction of the Ni_2Si precipitates in the specimen was measured at 4.43 wt.% (5.36 vol.%) using a calculated density of δ_D-Ni_2Si of 7.30 g/cm^3, and Cu of 8.94 g/cm^3. The measured composition and volume fraction were also consistent with those obtained from the Cu—Ni_2Si pseudo-binary phase diagram shown in Fig. 1.

Fig. 7 shows a bright-field TEM micrograph and corresponding SAED pattern for the specimens aged at 723 K for 240 h, as viewed from the $\langle 110\rangle_{Cu}$ incident beam direction. The bright-field TEM image presented in Fig. 7(a) shows the cellular component containing the fiber-shaped DPs in the copper solid-solution phase. The extra diffraction spots in the SAED pattern shown in Fig. 7(b) can be assigned to δ-Ni_2Si with an incident beam direction of $\langle 100\rangle_{\delta}$, which is consistent with the results shown in Fig. 6. Regarding the crystallographic orientation relationship (OR) with the matrix, Fig. 7(b) shows that the OR of the δ_D-Ni_2Si can be expressed as $\langle 100\rangle_{\delta D}//\langle 110\rangle_{Cu}$ and $(013)_{\delta D}//(111)_{Cu}$. Figs. 7(a) and (b) also show that the fiber-shaped DPs extend with an interface preferentially parallel to either the $(111)_{Cu}$ plane (or $(013)_{\delta D}$ plane as viewed from the DPs), although the fibers exhibit a slight wave in their growth.

We found that the crystal structure of the precipitates formed in Cu—Ni—Si alloys throughout the aging procedure is consistent with orthorhombic δ-Ni_2Si, regardless of whether the precipitates are nucleated and grown continuously within the grains or discontinuously at the grain boundaries. This is because the δ-Ni_2Si phase structure is the most stable, in terms of energy, of all the possible Ni—Si compound structures, such as β-Ni_3Si and $(Cu,Ni)_3Si$ [14]. Especially, in the case of the DPs formed in the specimen aged for a prolonged period, it should be reasonable for the crystal structure to belong to the stable and equilibrium phase of δ-Ni_2Si, according to the phase diagram shown in Fig. 1 or the ternary phase diagram [27]. The δ_D-Ni_2Si contains a small amount of Cu (shown in Table 2), which is also in good agreement with the phase diagram shown in Fig. 1. On the other hand, the δ_D-Ni_2Si deviates

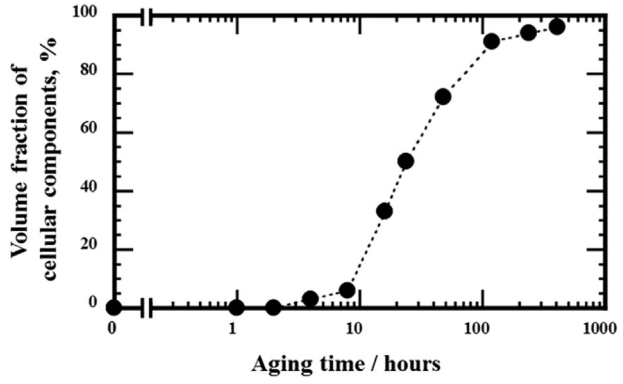

Fig. 4. Change in the volume fractions of cellular components by aging for the Cu-4.3 at.% Ni-2.2 at.% Si alloy specimens aged at 723 K; the values were measured by analyzing the FESEM images of the specimens.

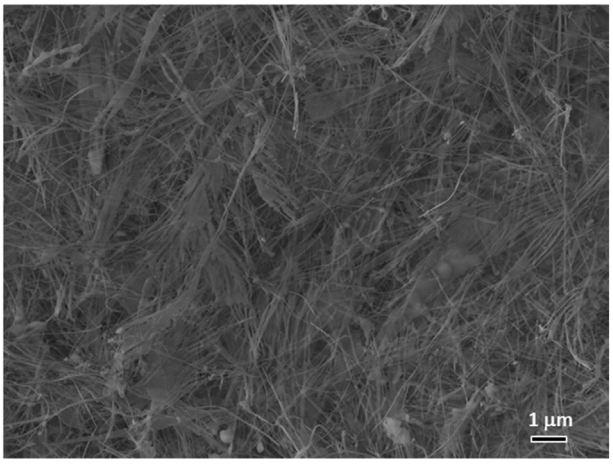

Fig. 5. Appearance of discontinuous precipitates separated from Cu-4.3 at.% Ni-2.2 at.% Si alloy specimens aged at 723 K for 240 h, using an extraction procedure by submerging in 7.0 mol/L nitric acid solution for 20 min at 273 K.

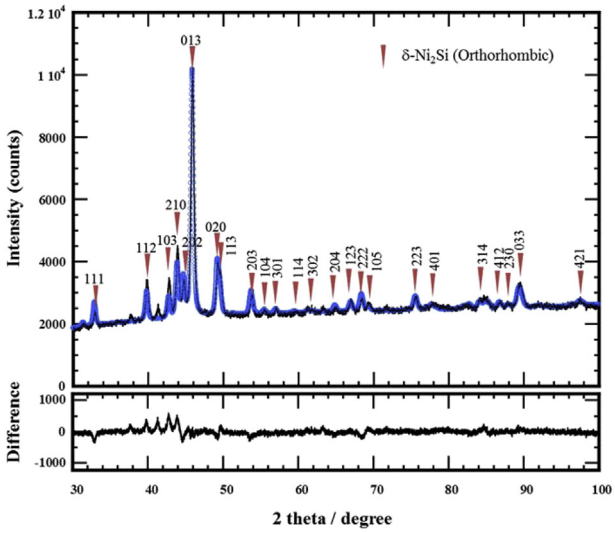

Fig. 6. X-ray diffraction patterns of insoluble residue separated by dissolution in 7.0-mol/L nitric acid at 273 K for 20 min from Cu-4.3 at.% Ni-2.2 at.% Si alloy specimens aged at 723 K for 240 h. The patterns measured and calculated using Rietveld analysis are indicated by the solid line and open circles, respectively. The difference between the measured and calculated intensities is shown at the bottom.

from the stoichiometric composition, being silicon-rich. This suggests that the δ-Ni_2Si intermetallic phase has some compositional extent at a low temperature of 723 K, which should be clarified in the future.

The crystallographic features of the fiber δ_D-Ni_2Si DPs are not the same as those of the fine disk-like δ_1-Ni_2Si CPs nucleated in the early aging stage, but are the same as those of the coarsened (but still nano-scaled) cigar-shaped δ_2-Ni_2Si CPs in the later aging stages [14]. This can be explained by a classic energy estimation; it is accepted that the free energy for precipitate nucleation, ΔG can be described as follows, when the interfacial energy, γ, of the precipitate/matrix interface is anisotropic:

$$\Delta G = V(\Delta Gv + \Delta Gs) + \Sigma Ai\gamma i \quad (1)$$

where V is the volume of the precipitate, ΔG_v is the volume free energy reduction upon precipitation, ΔG_s is the strain energy per unit volume, and A is the interface area. For the small precipitates (i.e., the value of V is small), the OR and habit plane should be controlled so as to minimize the total interfacial energy, $\Sigma A_i\gamma_i$, introduced by the lattice misfits between a particle and the matrix [28]. In the case of fine δ_1-Ni_2Si precipitates, the crystallographic OR is expressed as $\langle 010\rangle_{\delta 1}//\langle 110\rangle_{Cu}$, and $(001)_\delta//(001)_{Cu}$. Thus, the lattice misfit values between the δ_1-Ni_2Si and the matrix for the three principle directions of the precipitate are calculated as being 2.41% in the $\langle 100\rangle_{\delta 1}$ direction, 2.81% in the $\langle 010\rangle$ direction, and 8.26% in the $\langle 001\rangle_{\delta 1}$ direction, as reported by Hu et al. [14]. Therefore, the δ_1-Ni_2Si particles tend to be disk-shaped, since the growth in the $\langle 001\rangle_{\delta 1}$ direction is restricted due to the large misfit of 8.26% in this direction, and since there are much fewer misfits, of a similar magnitude, in the two principle ($\langle 100, 010\rangle$) directions in this plane.

For the coarse δ_2-Ni_2Si precipitates, the contribution of the $V(\Delta G_v + \Delta G_s)$ term is prominent. Thus, in the transformation from δ_1-Ni_2Si to δ_2-Ni_2Si, a small rotation of about 2.7° around the $\langle 110\rangle_{Cu}//\langle 100\rangle_{\delta 1}$ axes can reduce the strain energy, ΔG_s, by forming a broad interface, which is explained by the invariant line theory. Eventually, the disk-shaped δ_1-Ni_2Si transforms smoothly to cigar-shaped δ_2-Ni_2Si, such that the crystallographic OR between the δ_2-Ni_2Si and the matrix is expressed as $\langle 100\rangle_{\delta 2}//\langle 110\rangle_{Cu}$ and $(013)_{\delta 2}//(111)_{Cu}$.

The fiber δ_D-Ni_2Si discontinuous precipitates develop with the same crystallographic features as the coarse δ_2-Ni_2Si continuous precipitates. Therefore, we can assume that their growing mechanism is also the

Table 1
The lattice parameters of δ-Ni2Si.

Lattice parameters	Pure δ-Ni_2Si [17]	δ-Ni_2Si by CPs [13]	δ_D-Ni_2Si by DPs
A (nm)	0.50088	0.504 ± 0.005	0.499
B (nm)	0.37321	0.364 ± 0.005	0.372
C (nm)	0.70664	0.708 ± 0.005	0.703

Table 2
The elemental composition and volume fraction of the matrix and δ-Ni2Si precipitate phase in for the Cu-4.3 at.% Ni-2.2 at.% Si alloy specimen aged at 723 K for 240 h.

		Matrix	Precipitate
Composition, at.%	Cu	99.33 ± 0.18	0.77 ± 0.01
	Ni	0.67 ± 0.01	62.15 ± 0.29
	Si	<0.001	37.07 ± 0.22
Fraction	wt.%	95.81 ± 0.18	4.43 ± 0.02
	vol.%	94.64 ± 0.17	5.36 ± 0.02

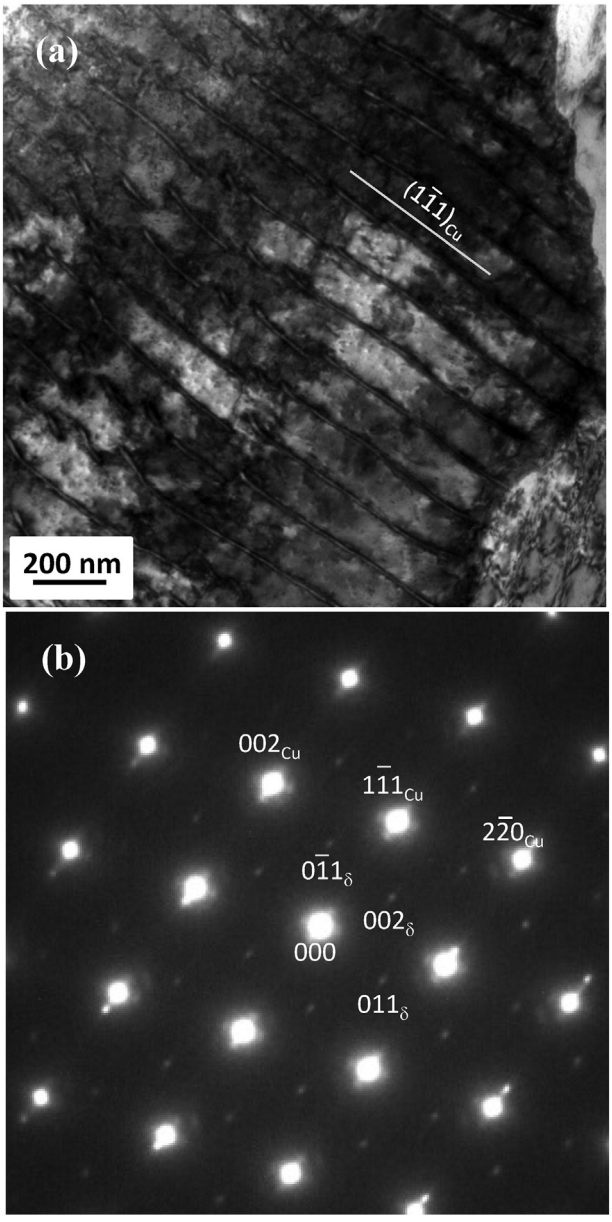

Fig. 7. Bright-field TEM image (a) and corresponding SAED pattern (b) of Cu-4.3 at.% Ni-2.2 at.% Si alloy specimens aged at 723 K for 240 h.

same as the coarse δ_2-Ni_2Si continuous precipitates, even though the nucleation manner is different. The δ_D-Ni_2Si DPs grow into a fiber-shape that is several μm in length, thus minimizing the total of the free energy for precipitate nucleation, ΔG. This is because the force driving the growth must be controlled by the volume free energy rather than the interfacial energy, in the same way as in the case of the δ_2-Ni_2Si precipitates.

3.3. Influence of DPs on hardness and conductivity

Fig. 8 shows the hardness and electrical conductivity as a function of the aging time for the specimen aged at 723 K. The age-hardening and conductivity responses of the specimen can be roughly divided into three stages: (I) the early stage of aging in which there is a rapid increase in the hardness, reaching a peak of approximately 270 Hv; (II) the subsequent stage of over-aging in which there is a rapid decrease in the hardness; and (III) the final stage, in which hardness and electrical conductivity are saturated after 240 h of aging.

In stage (II), since we can clearly distinguish the regions with the CPs or DPs as shown in Fig. 3, we can measure the individual hardness of each region. The hardness of the CPs and DPs is also plotted using open diamonds and squares, respectively, in Fig. 8(a). Considering only the hardness of the CP regions, once the maximum value of 270 Hv has been reached, the hardness decreases gradually as plotted by the open diamonds in Fig. 8(a). On the other hand, the local hardness of the cellular components containing the DPs was found to be around 145 Hv, which is much smaller than that of the region containing the CPs. Therefore, it is demonstrated that a rapid decrease in the hardness of the overall alloy was primarily due to the increase in the volume fraction of the cellular components, as shown in Fig. 4, through the consumption of the fine CPs. Thus, to let a conventional practical polycrystal alloy have ideal mechanical properties, it is necessary to suppress the nucleation and growth of the δ-Ni_2Si fibers at the grain boundaries. Efforts to control the characteristics of the grain boundaries by using thermomechanical processes and incorporating a fourth element, which affect the grain boundary energy, are currently underway.

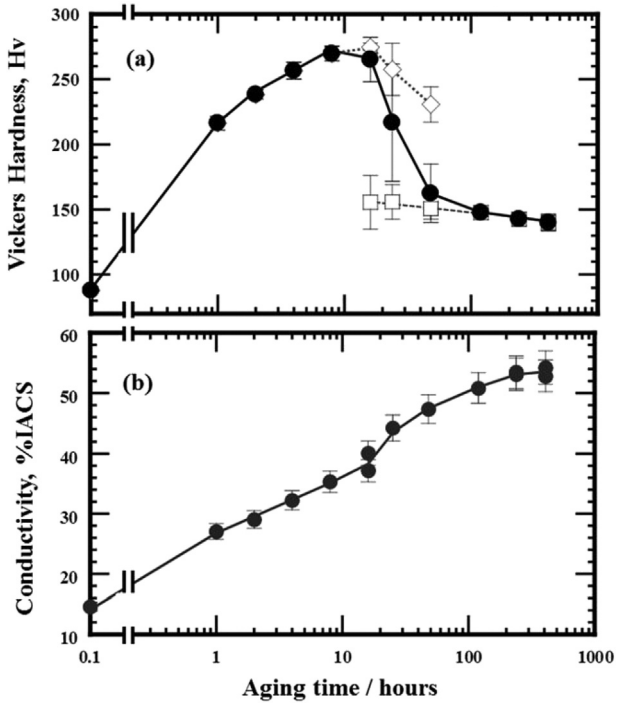

Fig. 8. Variations in Vickers hardness (a) and electrical conductivity as a function of aging time for Cu-4.3 at.% Ni-2.2 at.% Si alloy specimens aged at 723 K, indicated by solid circles. The open diamonds and squares indicate the hardness of the regions with the fine continuous precipitates and the cellular component containing discontinuous fiber precipitates, respectively.

The electrical conductivity increases gradually during aging, reaching saturation at 55% IACS in the final stage of aging. This is due to the depletion of the solute Ni and Si elements from the host copper phase by the formation of continuous and discontinuous precipitates. The saturated conductivity value of 55% IACS can also be explained, based on the equilibrium microstructure of the specimen aged for 240 h, as listed in Table 2, ignoring the concentration of Si in the copper matrix and the contribution of the δ-Ni_2Si phase because its conductivity will be much lower than that of the copper matrix. The electrical conductivity, σ, in a copper solid solution alloy can be approximated using Nordheim's rule [29,30]:

$$1/\sigma = \rho = \{\rho Cu + ACNi(1-CNi)\}VfCu \quad (2)$$

where, ρ and ρ_{Cu} are the resistivity of the specimen and pure copper at 293 K, respectively. Here, the value for the copper, ρ_{Cu}, is 1.724×10^{-8} Ωm. A is a constant depending on the solute Ni of 1.3×10^{-8} Ωm/at.% in the host Cu, and C_{Ni} is the atomic fraction of the solute Ni. Vf_{Cu} is the volume fraction of Cu matrix in the specimen, which is listed in Table 2. Therefore, the value of the conductivity of the alloy, σ, was estimated to be (60 ± 2)% IACS, which was in reasonably good agreement with the measured value.

4. Conclusions

The discontinuous precipitate formed in the Cu-4.3 Ni-2.2 Si (in at.%) alloys during aging has a structure corresponding to δ-Ni_2Si with an orthorhombic structure. The δ-Ni_2Si discontinuous precipitates exhibit a fiber-shape in the cellular components at the end of the early stage of aging (4 h at 723 K), and then grow quickly, reaching several μm in length by occupying an entire grain. The cellular components containing fiber δ-Ni_2Si discontinuous precipitates develop throughout the specimen in the final stage of aging, accompanying the replacement of fine δ-Ni_2Si continuous precipitates.

The δ-Ni_2Si discontinuous precipitates preferentially extend across the $\{111\}_{Cu}$ matrix plane while exhibiting a slight wave. The crystal orientation relationship is expressed as $\langle 100\rangle_\delta // (110)_{Cu}$ and $(013)_\delta // (111)_{Cu}$, which differs from the δ-Ni_2Si discontinuous precipitates formed in the early stages of aging. The δ-Ni_2Si discontinuous precipitates were found to contain a small amount of copper, while the measured Ni/Si ratio was 1.68, being somewhat less than the stoichiometric composition of 2.0.

We confirmed that the formation of coarse δ-Ni_2Si fibers in the cellular components is detrimental to alloy hardening, because the fine δ-Ni_2Si continuous precipitates that were favorable for hardening are replaced with coarse δ-Ni_2Si discontinuous precipitates that were unfavorable for hardening. On the other hand, the formation of continuous and discontinuous precipitates results in a significant increase in the electrical conductivity, because the solute Ni and Si content in the host copper matrix is reduced and finally falls to 0.67 at.% Ni and <0.001 at.% Si.

Acknowledgements

The authors are grateful to Prof. S. Hanada and Prof. N. Masahashi of the Institute for Materials Research (IMR) of Tohoku University, and Dr. A. Sugarawa, Dr. F. Sasaki, and Mr. H. Suda of DOWA METALTECH Co., Ltd. for their useful discussions and comments. The authors also thank Mr. E. Aoyagi and M. Ishikuro of IMR for their technical assistance. Financial support was provided by the Japan Society for the Promotion of Science (JSPS) as a Grant-in-Aid for Scientific Research (C) (No. 26420663) and by the Japan Copper and Brass Association (2014 to 2015).

References

[1] Z. Rdzawski, J. Stobrawa, Thermomechanical processing of Cu–Ni–Si–Cr–Mg alloy, Mater. Sci. Technol. 9 (1993) 142–149.
[2] F. Huang, J. Ma, H.L. Ning, Y.W. Cao, Z. Geng, Precipitation in Cu–Ni–Si–Zn alloy for lead frame, Mater. Lett. 57 (2003) 2135–2139.
[3] R. Monzen, C. Watanabe, Microstructure and mechanical properties Cu–Ni–Si alloys, Mater Sci Eng A 483-483 (2014) 117–119.
[4] S. Lee, H. Matsunaga, X. Sauvage, Z. Horita, Strengthening of Cu–Ni–Si alloy using high-pressure torsion and aging, Mater Charact 90 (2014) 62–70.
[5] E.M. Sokolovskaya, O.I. Chechernikova, E.I. Gladyshevskii, O.I. Bodak, The Ni–Cu–Si system, Russ. Metall. 6 (1973) 114–118.
[6] M.G. Corson, Copper hardened by new method: what the Corson alloys are stronger cable wire possible-many uses suggested-silicon–aluminum and silver–silicon alloys, Iron Age 119 (1927) 421–424.
[7] M.G. Corson, Electrical conductor alloys, Electr. World 89 (1927) 137–139.
[8] W.D. Robertson, E.G. Grenier, V.F. Nole, The structure and associated properties of an age hardening copper alloy, Trans. Metall. Soc. AIME 221 (1961) 503–512.
[9] S.A. Lockyer, F.W. Noble, Precipitate structure in a Cu–Ni–Si ally, J Mater Sci 29 (1994) 218–226.
[10] D.M. Zhao, Q.M. Dong, P. Liu, B.X. Kang, J.L. Huang, Z.H. Jin, Aging behavior of Cu–Ni–Si alloy, Mater Sci Eng A 361 (2003) 93–99.
[11] Y. Takahashi, T. Sanada, S. Sato, T. Okajima, K. Shinoda, S. Suzuki, SAXS and XAFS characterization of precipitates in a high-performance Cu–Ni–Si alloy, Mater Trans 48 (2007) 101–104.
[12] E. Donoso, R. Espinoza, M.J. Dianez, J.M. Criado, Microcalorimetric study of the annealing hardening mechanism of a Cu–2.8Ni–1.4Si (at.%) alloy, Mater. Sci. Eng. A 556 (2012) 612–616.
[13] J. Yan-lin, W. Ming-pu, C. Chang, D. Qi-yi, W. Shan, L. Zhou, Orientation and diffraction patterns of δ–Ni2Si precipitates in Cu–Ni–Si alloy, J. Alloys Compd. 557 (2013) 147–151.
[14] T. Hu, J.H. Chen, J.Z. Liu, Z.R. Liu, C.L. Wu, The crystallographic and morphological evolution of the strengthening precipitates in CuNiSi alloys, Acta Mater 61 (2013) 1210–1219.
[15] H. Azzeddine, B. Mehdi, L. Hennet, D. Thiaudière, B. Alili, M. Kawasaki, D. Bradai, T.G. Langdon, An in situ synchrotron X-ray diffraction study of precipitation kinetics in a severely deformed Cu–Ni–Si alloy, Mater Sci Eng A 597 (2014) 288–294.
[16] K. Toman, The structure of Ni2Si, Acta Crystallogr 5 (1952) 329–331.
[17] F. Bosselet, J.C. Viala, C. Colon, B.F. Mentzen, J. Bouix, Solid state solubility of aluminum in the δ–Ni2Si nickel silicide, Mater Sci Eng A 167 (1993) 147–154.
[18] H. Tsubakino, R. Nozato, H. Hagiwara, Discontinuous precipitation in Cu2.1 mass% Be Alloy, Trans. Jpn. Inst. Metals 22 (1981) 153–162.
[19] H. Tsubakino, Discontinuous precipitation in a Cu–Sn Alloy, Metallography. 17 (1984) 371–382.
[20] R. Monzen, C. Watanabe, D. Mino, S. Saida, Initiation and growth of the discontinuous precipitation reaction at ⟨011⟩ symmetric tilt boundaries in Cu–Be alloy bicrystals, Acta Mater 53 (2005) 1253–1261.
[21] S. Semboshi, M. Ishikuro, S. Sato, K. Wagatsuma, A. Iwase, T. Takasugi, Investigation of precipitation behavior in age-hardenable Cu–Ti alloys by an extraction-based approach, Metall. Mater. Trans. A 45 (2014) 3401–3411.
[22] Q. Lei, Z. Li, M.P. Wang, L. Zhang, S. Gong, Z. Xiao, Z.Y. Pan, Phase transformation behavior in a Cu–8.0Ni–1.8Si alloy, J. Alloys Compd. 509 (2011) 3617–3622.
[23] E. Lee, K. Euh, S.Z. Han, S.H. Lim, J.H. Lee, S.S. Kim, Tensile and electrical properties of direct aged Cu–Ni–Si–x%Ti alloys, Metall. Mater. Int. 19 (2013) 1183–1188.
[24] C. Watanabe, R. Monzen, K. Higashimine, Discontinuous precipitation in a Cu-4 mass% Ni-0.95 mass% Si alloy, Proceedings of an International Conference on Solid-Solid Phase Transformations in Inorganic Materials, 1 2005, pp. 713–718.
[25] S. Semboshi, M. Ishikuro, S. Sato, K. Wagatsuma, T. Takasugi, Extraction of precipitates from age-hardenable Cu–Ti alloy, Mater Charact 82 (2013) 23–31.
[26] T. Souma, M. Ohtaki, Synthesis and Rietveld analysis of Zn4-xCdxSb3 bulk crystals in the Zn-rich region, J. Alloys Compd. 413 (2006) 289–297.
[27] X. Liu, S. Xiang, S. Yang, R. Shi, C. Wang, Experimental investigation of phase equilibria in the Cu–Ni–Si ternary system, J. Alloys Compd. 578 (2013) 439–447.
[28] Porter DA, Easterling KE. Phase Transformations in Metals and Alloys. 2nd ed. CRC Press; 2004.
[29] J. Miyake, M.E. Fine, Electrical conductivity versus strength in a precipitation hardened alloy, Acta Metall 40 (1992) 733–741.
[30] S. Semboshi, T.J. Konno, Effect of aging in hydrogen atmosphere on electrical conductivity of Cu-3 at.% Ti alloy, J. Mater. Res. 23 (2008) 473–477.